A Feedback Linearization Based Control Strategy for VSC-HVDC Transmission Converters

LI SHUANG, WANG ZHIXIN, WANG GUOQIANG
Department of Electrical Engineering
Shanghai Jiaotong University
No.800 Dong Chuan Road, Shanghai 200240
P.R. CHINA
cooleels@126.com

Abstract: - In this paper, a global stability and robust nonlinear controller for VSC-HVDC transmission Converters applying input-output linearization (IOL) techniques is proposed. The feedback linearization based nonlinear differential-geometric techniques is used to cancel nonlinearities and decouple the input control variables. Global tracking capability with zero steady-state error of the voltage loop has been achieved by zero-dynamic control. Also, there is no derivative calculation required and measurement of load current is not needed. The proposed controller is of many advantages compared with the traditional control strategies, such as global stability, fast dc-bus voltage response, robust against parameter uncertainties and decoupled dynamical d-q current loops. Comprehensive time-domain computer simulations within MATLAB/SIMULINK have been carried out to confirm the proposed control scheme.

Key-Words: - Voltage-Source Converters (VSC)-HVDC; Nonlinear Control; Feedback Linearization; Input-Output Linearization (IOL); Differential-Geometric

1 Introduction

Three-phase pulse-width modulation (PWM) voltage-source converters (VSC)-HVDC link using the state-of-the-art power electronic devices, such as insulated-gate bipolar transistor (IGBT), have motivated increasing attentions and studies in recent years [1] [2]. As compared to traditional converters, the PWM-VSC has the attractive features such as almost sinusoidal input currents, controllable input power factor, constant dc-bus voltage and bidirectional power flow ability with separately control of active and reactive power [3] [4]. All these features make VSC-HVDC systems suitable for connecting renewable sources to the main grid, especially on offshore wind farms [5-7].

Many research have been done from the control point of view[8] [9] [10] [11] [12] [13] [14], most of those results relay on either using small-signal stability or linearized models with compensation. Their performances will retain under certain conditions such as limited operation range and large dc-bus capacitance [15]. Certainly, it is difficult to achieve ideal control effects with linear control theories for the multivariable control inputs and highly coupled nonlinearity of the VSC-HVDC. By dint of its structure, nonlinear control theories based on the input-output linearization (IOL) have been developed over recent years and achieved considerable successes [16] [17] [18]. The main achievement of this nonlinear control technique was the decoupling and linearization of the synchronous d-q axes dynamics in VSC. However, its involved mathematical intricateness has somehow constrained the widespread usage of this technique. Notwithstanding, thanks to the development of floating point based digital-signal-processor (DSP) and advanced control strategies, upon which IOL with nonlinear differential-geometric techniques [19] [20] have been one of the most essential tools for nonlinear system control. The major merit of these techniques is that one can find a global feedback law to linearize and decouple multi-input multi-output (MIMO) nonlinear system where regular linear design methods can be applied [21] [22].

This paper presents thence a nonlinear mathematical model of the VSC-HVDC transmission converters in the synchronous reference frame and its controller using IOL technique developed from differential-geometric theory, thus expanding the usage of this particular technique. Also, it is shown that the global tracking capability with zero steady-state error of the voltage loop can be achieved. For physical realization of the PI outer-loop control, the suitable parameters of PI controller are derived. In this paper, several computer simulations with MATLAB®/SIMULINK® are carried out and results are presented to test the robustness of the designed controller.

2 Mathematical modeling of the VSC-HVDC transmission converters

Usually, two VSC stations constitute a typical VSC-HVDC system. For one station on the offshore wind farm side operates as the rectifier station whereas the onshore main grid side operates as the inverter station. The topologies of the stations are symmetry, so the power circuit of one station (take rectifier station for example) is shown in Fig. 1. It is assumed that the VSC operates under a balanced three phase ac source, and resistive load R_L is connected to the output terminal and neglected the resistance of the power switches. So the dynamic equations of the PWM VSC in the rotating d-q frame can be expressed as follows [8] [18] [23] [24] :

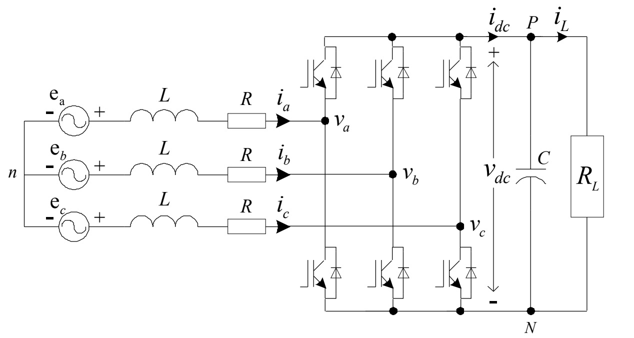

Fig.1 Power circuit of the three-phase PWM VSC.

$$L\frac{di_d}{dt} = -Ri_d - \omega Li_q - \upsilon_{dc}d_d + e_d \tag{1}$$

$$L\frac{di_q}{dt} = -Ri_q + \omega Li_d - \upsilon_{dc}d_q \tag{2}$$

$$C\frac{d\upsilon_{dc}}{dt} = \frac{3}{2}(i_d d_d + i_q d_q) - i_L \tag{3}$$

where:

e_d amplitude of the source phase voltage in d axis (under a balanced three phase supply $e_d = E_m$);

$d_{d,q}$ switching functions;

C dc-link capacitance;

R, L resistance and inductance of the boosting inductor

In the equations (1)-(3), the state vector can be defined as $x = [x_1 \quad x_2 \quad x_3]^T = [i_d \quad i_q \quad \upsilon_{dc}]^T$. The control input vector $u = \begin{bmatrix} u_d & u_q \end{bmatrix}^T = \begin{bmatrix} d_d & d_q \end{bmatrix}^T$ is the switching functions in synchronous rotating d-q coordinate.

Equations (1)-(3) and the state-space functions both show the nonlinear nature of the VSC systems, for the control input u multiplied by the state variables. The coupling between the components on axis d and axis q of the current sets an initial problem in constructing a system controller. Usually, controller is based on the principle of cascade regulation. The internal loop imposes sinusoidal shape of the line currents and the external loop maintains the capacitive voltage x_3 at a constant reference value V_{ref}. With this type of converter, $x_2(i_q)$ is regulated to zero because of e_q equal zero under a balanced three phase supply.

3 Feedback linearization

A brief theoretical background of feedback linearization is herein presented before presenting the derivation of control schemes, whose detailed description can be found in [16] [17] [19]. Consider the following multiple-input multiple-output (MIMO) nonlinear system

$$\dot{x} = f(x) + G(x)u \tag{4}$$

$$y = h(x) \tag{5}$$

where x is an $n \times 1$ state vector, y is $m \times 1$ output vector, $f(x)$ and $h(x)$ are n[th]-order smooth vector fields, $G(x)$ is an $n \times m$ matrix of smooth vector field columns g_i, and u is the $m \times 1$ control input vector. An approach to obtain the IOL of the MIMO system is to differentiate the output y of the system until the inputs appear. The smallest number of derivatives required for that γ_i is called the relative degree of that particular output.

These derivatives may be expressed as follows:

$$y_i^{(\gamma_i)} = L_f^{\gamma_i} h_i + \sum_{j=1}^{m} L_{g_j} L_f^{\gamma_i - 1} h_i u_j \tag{6}$$

where $L_{g_j} L_f^{\gamma_i-1} h_i \neq 0$ for at least one in (6) if the previously mentioned condition is complied. The Lie derivative for any scalar function of h is defined as $L_f h = \nabla h \cdot f$, thus, $L_f^i h = L_f L_f^{i-1} h = \nabla(L_f^{i-1} h) f$ is defined recursively for any positive integer i.

After performing the process to each output state variable as equation (6), the following system of differential equations is obtained:

$$\begin{bmatrix} y_1^{(\gamma_1)} \\ \vdots \\ y_m^{(\gamma_m)} \end{bmatrix} = \begin{bmatrix} L_f^{\gamma_1} h_1(x) \\ \vdots \\ L_f^{\gamma_m} h_m(x) \end{bmatrix} + E(x) \begin{bmatrix} u_1 \\ \vdots \\ u_m \end{bmatrix} \tag{7}$$

or equivalently

$$y = A(x) + E(x)u \tag{8}$$

where the $m \times m$ decoupling matrix $E(x)$ was defined as:

$$E(x) = \begin{bmatrix} L_{g_1} L_f^{\gamma_1 - 1} h_1(x) & \cdots & L_{g_m} L_f^{\gamma_1 - 1} h_1(x) \\ \vdots & \ddots & \vdots \\ L_{g_1} L_f^{\gamma_m - 1} h_m(x) & \cdots & L_{g_m} L_f^{\gamma_m - 1} h_m(x) \end{bmatrix} \tag{9}$$

And then, if $E(x)$ is nonsingular, the new transformed system with IOL can now be written as

$$u = E^{-1}(x)\left[\upsilon - A(x)\right] \tag{10}$$

where υ is a dummy input vector. Substituting equation (10) into (8) results in a linear differential relation between the output y and the new input υ

$$\begin{bmatrix} y_1^{(\gamma_1)} \\ \vdots \\ y_m^{(\gamma_m)} \\ \dot{z} \end{bmatrix} = \begin{bmatrix} \upsilon_1 \\ \vdots \\ \upsilon_m \\ a(z, y, \upsilon) \end{bmatrix} \tag{11}$$

which is a linear differential relation between each input-output pair. Furthermore, we can see each input υ_i only affects its correspondent output $y_i^{(\gamma_i)}$, so it is decoupled linear relation.

Now suppose that tracking of the constant output reference $y^* = \begin{bmatrix} y_1^* & \cdots & y_m^* \end{bmatrix}^T$ is required, by setting the auxiliary feedback [1]

$$\begin{cases} \upsilon_1 = -k_{1(\gamma_1-1)} y_1^{(\gamma_1-1)} - \cdots - k_{11} y_1^{(1)} - k_{10}\left(y_1 - y_1^*\right) \\ \vdots \qquad \vdots \qquad \vdots \qquad \vdots \\ \upsilon_m = -k_{m(\gamma_m-1)} y_m^{(\gamma_m-1)} - \cdots - k_{m1} y_m^{(1)} - k_{m0}\left(y_m - y_m^*\right) \end{cases} \tag{12}$$

for some positive constants $k_{ij}, i = 1, \ldots, m; j = 1, \ldots, \gamma_i$, the closed-loop error dynamics show as follows

$$\begin{cases} e_1^{\gamma_1} + k_{1(\gamma_1-1)} e_1^{(\gamma_1-1)} + \cdots + k_{11} e_1^{(1)} + k_{10} e_1 = 0 \\ \vdots \qquad \vdots \\ e_m^{\gamma_m} + k_{m(\gamma_m-1)} e_m^{(\gamma_m-1)} + \cdots + k_{m1} e_m^{(1)} + k_{m0} e_m = 0 \end{cases} \tag{13}$$

$$\dot{z} = a(z, e + y^*, \xi) \tag{14}$$

where $\zeta = \left[y_1^{(\gamma_1-1)}, \ldots, y_1^{(1)} \quad , \cdots, \quad y_m^{(\gamma_m-1)}, \ldots, y_m^{(1)} \right]^T$ and $e_i = y_i - y_i^*, i = 1, \cdots, m$. It is easy to choose appropriate k_{ij} to make the error dynamics stable and track the reference y^* by usual linear pole placement technique. The internal dynamic equation (14) when tracking error e vanishes is called the zero dynamics [17].

$$\dot{z} = a(z, y^*, 0) \tag{15}$$

With (13) one can stabilize the error dynamic by setting suitable linear state feedback. On the other hand, the equilibrium stability of the zero dynamics (15) determines the equilibrium stability of the transformed system (13), (14) under IOL laws (10), (12) [19]. When the zero dynamics is asymptotically stable, the nonlinear system is minimum-phase [16].

4 IOL and current inner-loop control of the PWM VSC

The feedback linearization is particularly useful in power electronics to track the nonlinear problem, where a nonlinear process is transformed into a linear one by forcing the output to follow the input in a closed-loop fashion. According to the aforementioned theory of IOL, we will derive the cascaded current control scheme here. Meanwhile, the dc-bus voltage of the VSC can be controlled by choosing two different dummy output variable [22].

Specialized to the two-input two-output nonlinear state equations characterizing the PWM VSC，we can substitute equations (1-3) into (4) with $n = 3$, $m = 2$ to get

$$\begin{bmatrix} \dot{x}_1 \\ \dot{x}_2 \\ \dot{x}_3 \end{bmatrix} = \begin{bmatrix} -\frac{R}{L} x_1 - \omega x_2 + \frac{E_m}{L} \\ \omega x_1 - \frac{R}{L} x_2 \\ -\frac{i_L}{C} \end{bmatrix} + \begin{bmatrix} -\frac{1}{L} x_3 & 0 \\ 0 & -\frac{1}{L} x_3 \\ \frac{3}{2C} x_1 & \frac{3}{2C} x_2 \end{bmatrix} \begin{bmatrix} u_d \\ u_q \end{bmatrix} \tag{16}$$

Applying the theory of IOL, it is nature to choose $y = [x_1 \quad x_2]^T = [i_d \quad i_q]^T$ as the dummy output. Obviously, the reference must be set to $y^* = [i_d \quad 0]^T$, when the q axis current component

$x_2 = 0$ under unity power factor condition. The dc-bus voltage x_3 will be regulate to a desired value V_{ref} indirectly when the output i_d tracking I_d^*.

From the steady-state solution of (1)-(3) with desired voltage reference V_{ref}, one could determine the desired current command I_d^* [25], as follows:

$$E_m = RI_d^* + V_{ref} D_d \tag{17}$$

$$0 = \omega L I_d^* - V_{ref} D_q \tag{18}$$

$$0 = \frac{3}{2} I_d^* d_d - I_L \tag{19}$$

where D_d, D_q and $I_L = V_{ref}/R_L$ are the steady-state values of the switching function and output load current respectively. From (17) and (19) we can get the steady-state input line current

$$I_d^* = \frac{1}{2}\left[\frac{E_m}{R} \pm \sqrt{\left(\frac{E_m}{R}\right)^2 - \frac{8V_{ref} I_L}{3R}}\right] \tag{20}$$

As discussed in [22], the current reference command should choose the smaller one, so

$$I_d^* = \frac{1}{2}\left[\frac{E_m}{R} - \sqrt{\left(\frac{E_m}{R}\right)^2 - \frac{8V_{ref} I_L}{3R}}\right] \tag{21}$$

Applying the IOL method presents in previous section, the feedback equation is

$$\begin{bmatrix} D_d \\ D_q \end{bmatrix} = \begin{bmatrix} -\frac{1}{L}x_3 & 0 \\ 0 & -\frac{1}{L}x_3 \end{bmatrix}^{-1} \cdot \left(\upsilon - \begin{bmatrix} \frac{E_m}{L} - \frac{R}{L}x_1 - \omega x_2 \\ \omega x_1 - \frac{R}{L}x_2 \end{bmatrix} \right) \tag{22}$$

$$\upsilon = \begin{bmatrix} -k_{10}\left(y_1 - I_d^*\right) \\ -k_{20} y_2 \end{bmatrix} \tag{23}$$

Thus, we render the nonlinear VSC system in the linearized form of (13) and (14) with $z = x_3$ and the relative degrees $\gamma_i = 1, i = 1,2$, substitute equations (22) and (23) to (14) to get the internal dynamics as

$$\dot{x}_3 = -\frac{3}{2Cx_3}\{x_1\left[Rx_1 + \omega L x_2 - E_m + Lk_{10}\left(I_d^* - x_1\right)\right] \\ -x_2\left[Rx_2 - \omega L x_1 - Lk_{20}x_2\right]\} - \frac{i_L}{C} \tag{24}$$

Let the tracking error vector $e \to 0$, by $x_1 \to I_d^*$ $x_2 \to 0$ and $x_3 \to \upsilon_{ref}$ then the ideal energy conservative relation is as follow:

$$\frac{\upsilon_{ref}^2}{R_L} = \frac{3}{2}\left[E_m I_d^* - R(I_d^*)^2\right] \tag{25}$$

In the same time, with equation (24) and (25), the zero dynamics between ac and dc side is shown below

$$\dot{x}_3 = \frac{\left(\upsilon_{ref}^2 - x_3^2\right)}{R_L C x_3} \tag{26}$$

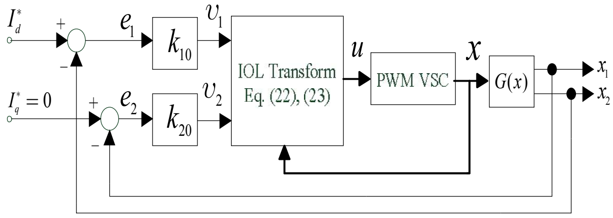

Fig. 2 VSC Current controller block diagram using IOL.

The stability of the equilibrium point of the zero dynamics (26) determines the system stability. As discussed in [22] both of roots $x_3^* = \pm\upsilon_{ref}$ are stable. In actual control scheme the initial dc-bus voltage is positive, therefore, this strategy used here can achieve the desired dc-bus reference voltage υ_{ref}. The block diagram of this current control scheme is shown in Fig. 2, in which the VSC model is linearized and removed the cross-coupling between d and q current dynamics.

5 Zero dynamics and Out-loop Control of the dc-bus voltage

As shown in (21), the dc-bus voltage will track the setting reference value V_{ref} when regulating the d-axis current to a desired point I_d^* by the zero dynamics (26). Albeit, these parasitical elements exist in the power circuit and temperature / aging cause parameters variation which show the nonlinear, especially the load disturbance may lead to zero steady-state error in dc-bus output. As a consequence, the out-loop controller should be devised to regulate the dc-bus voltage.

With reference to (25), we can setup an observer for the zero dynamics in the follow form

$$\dot{x}_3 = \frac{\Psi(i_d^*)}{R_L C x_3} - \frac{x_3}{R_L C} \tag{27}$$

where

$$\Psi(i_d^*) = \frac{3}{2} R_L \left[E_m i_d^* - R i_d^{*2} \right] \quad (28)$$

Substituting the nonlinear transform $\delta = x_3^2$ to (27), an almost linearized zero dynamics can be obtained

$$\dot{\delta} = \sigma[\Psi(i_d^*) - \delta] \quad (29)$$

where $\sigma = 2/R_L C$. In order to get robust dynamic performance, we employ the traditional PI controller to regulate the d-axis current reference as follow

$$i_d^* = k_P(\upsilon_{ref}^2 - \delta) + k_I \int (\upsilon_{ref}^2 - \delta) dt \quad (30)$$

where the relation between k_P and k_I have been discussed in [22] as

$$k_P > k_I / \sigma_{\min} \quad (31)$$

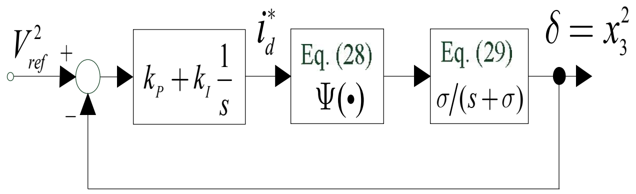

Fig.3 Block diagram of the dc-bus voltage control loop.

The controlled zero dynamics scheme is depicted in Fig. 3. Combining Fig. 2 and Fig. 3, we obtain the cascaded control scheme for the VSC, shown in Fig. 4.

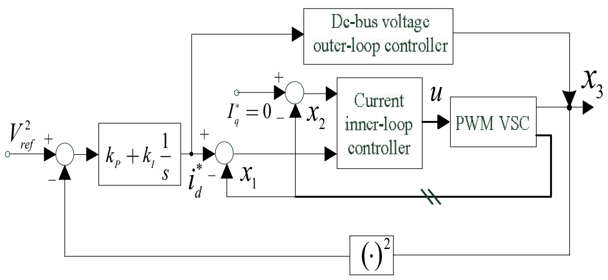

Fig.4 Block diagram of the cascaded controller for the PWM VSC.

The power rating of VSC-HVDC system restricts the maximum amplitude of the line currents. Meanwhile expression (21) determines the maximum output dc current if I_d^* exist a real solution

$$\left(\frac{E_m}{R} \right)^2 - \frac{8 V_{ref} I_L}{3R} \geq 0 \quad (32)$$

So, $I_{L\_\max} = 3E_m^2 / 8RV_{ref}$. It is obvious that the upper bound on the amplitude of the line currents is $I_d^* \leq E_m / 2R$, and lower limit can be obtained from equation (28) as $I_{L\_\min} = (1-\sqrt{2})E_m / 2R$. For the reason of symmetric of the VSC-HVDC stations, the maximum dc current in inverter station could be set to $I_{L\_\max\_rev} = -3E_m^2 / 8RV_{ref}$. It is obvious that the stability and robust control of the VSC system is improved.

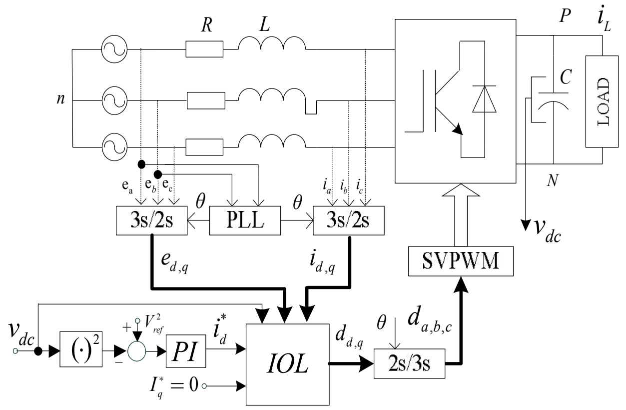

Fig.5 Nonlinear control of PWM VSC.

6 Simulation results and discussions

The proposed IOL nonlinear controller is tested in MATLAB®/SIMULINK® in order to demonstrate the validity of the control methodology. The control scheme of offshore rectifier station is shown in Fig. 5. The onshore inverter station is a symmetrical topology as shown in Fig. 6. Table 1 lists the parameters of the simulation model.

TABEL 1
Specifications of the PWM VSC in the simulation.

Power rating	500kVA
Source Voltage E_m	10kV
dc-bus voltage V_{ref}	20kV
Line inductor L	13mH
Inductor resistance R	0.4Ω
dc-bus capacitor C	1500uF
Line frequency ω	$100\pi rad/s$
PWM carrier frequency	2kHz

For a two-terminal VSC transmission system, as depicted in Fig. 6, normally one converter controls the DC voltage, namely the DC voltage controller (DCVC), and the other controls the active power, namely the active power controller (APC). The DCVC can operate as a rectifier or an inverter and the same applies to the APC, which are independent of the power transfer direction. Fig. 7 shows steady-state waveforms of the DCVC and APC with the proposed IOL cascaded-control scheme. Fig. 7(a) and (b) depict the converter operating at unity power factor. The advantage is obvious that it has little THD and low harmonics compared the result in Fig. 8 which was under traditional PI control scheme.

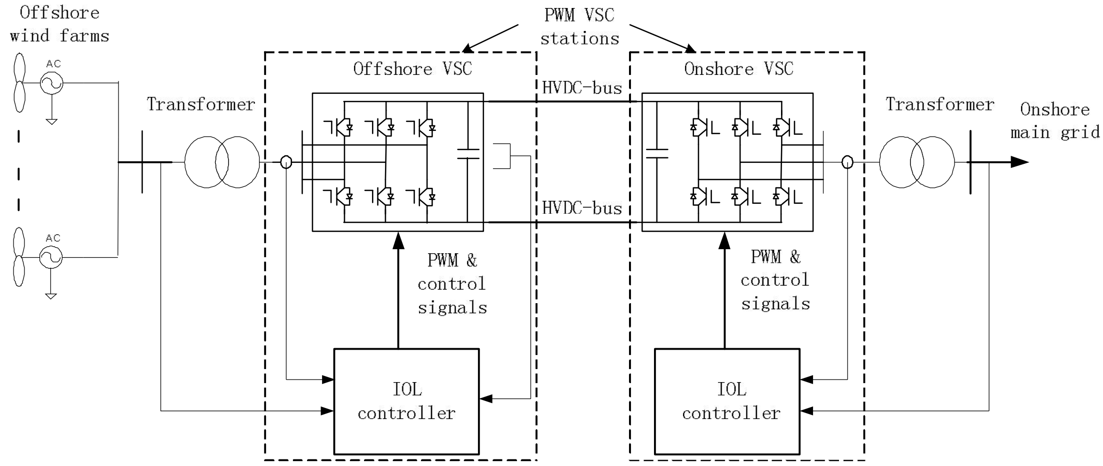

Fig.6 Block diagram of 500kVA VSC-HVDC.

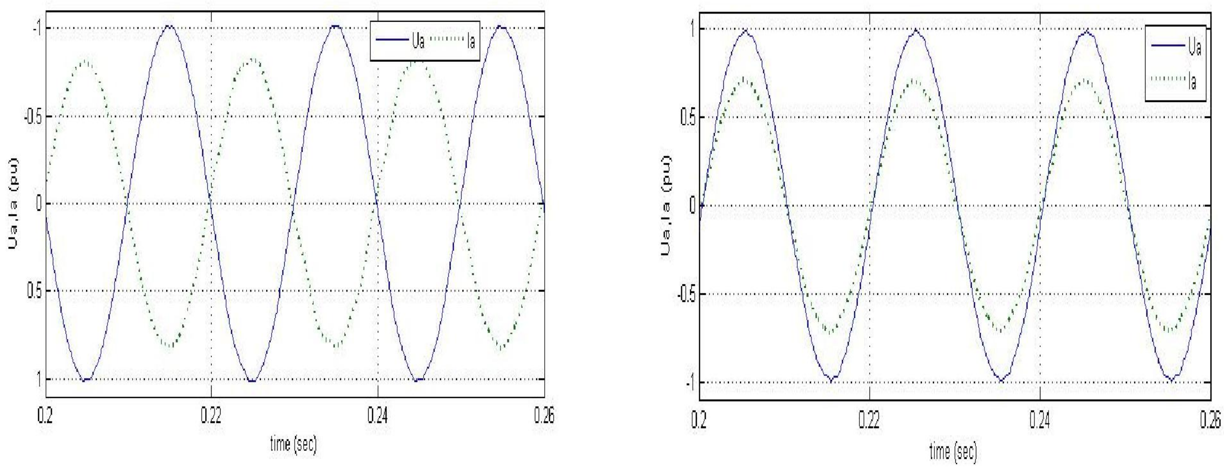

(a) (b)

Fig. 7 Ac side responses in steady-state under IOL control. (a) Inverter station. (b) Rectifier station.

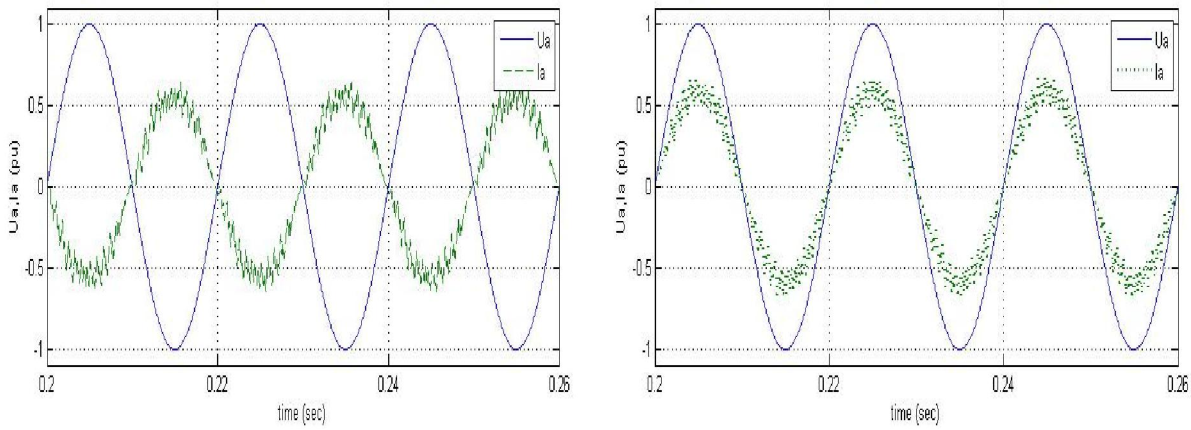

(a) (b)

Fig. 8 Ac side responses in steady-state under PI control. (a) Inverter station. (b) Rectifier station.

In Fig. 9, smaller overshoot and fast stabilization can be achieved under IOL control, compared to the traditional PI control. Fig. 10 shows when the setting point of the dc-bus voltage changes, between 0.4s~0.7s, the simulation model can track the new reference fast. The d-axis current changes at the beginning and the end of the voltage reference change, meanwhile the q-axis current only have negligible changes in the transient responses for some other uncertainty perturbations in the system. It can be shown the feature of current decoupling, and fast dc-bus voltage tracking property.

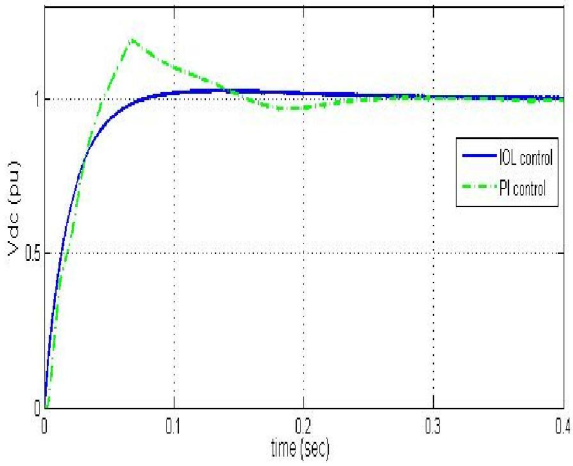

Fig. 9 Dc-bus steady-state responses under PI and IOL control scheme.

Fig. 11 shows the dynamic of the transmission active power step changes at 0.4s. Fig. 11 (a) and (b) show the dc-link voltage and current transient of the active power step change. With the proposed zero dynamic controller on the outer-loop, the influence to the dc-bus voltage is slight. And with a fast current tracking ability in the inner current loop, the d-axis current are regulated to the new setting point.

Fig. 12 is the situation of power flow reverse suddenly at 0.4s, where the DCVC and APC working conditions (inverting or rectifying) interchange with each other. The waveform of the dc-bus voltage and current, d, q axis currents, line voltage and current under a sudden change in the active power from 0.5pu to -0.5pu are shown in Fig. 12 (a)-(d)

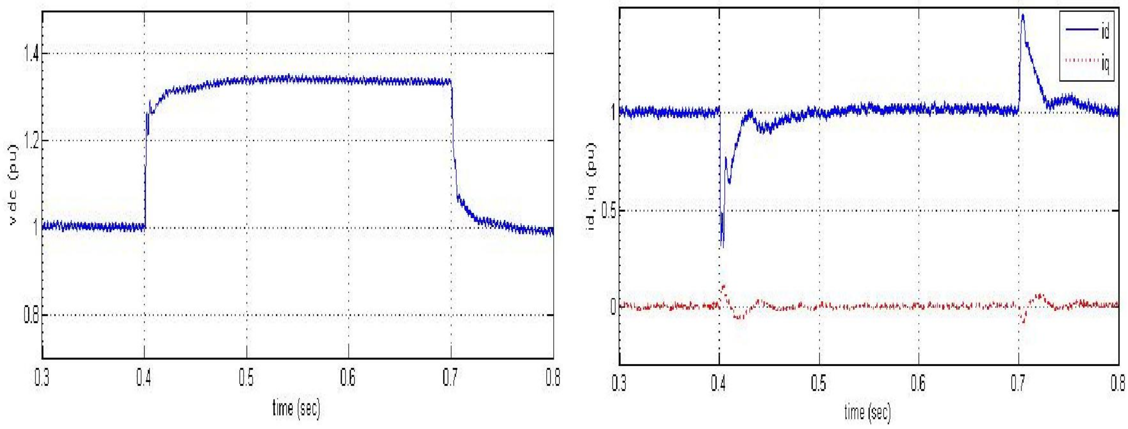

(a) (b)

Fig. 10 Voltage and current transient responses for dc-voltage reference changes. (a) Step changes in dc-bus voltage reference. (b) Decoupled d-q axis currents.

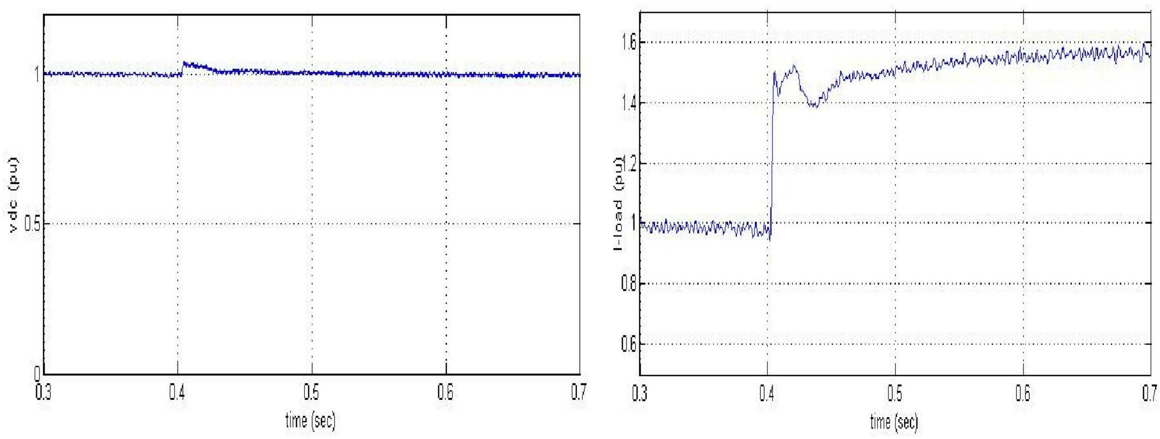

(a) (b)

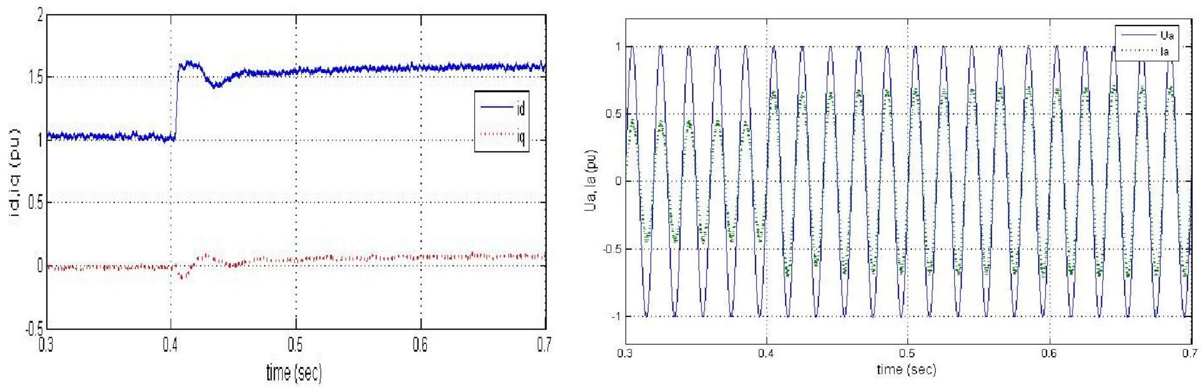

(c) (d)

Fig. 11 Responses to step changes in active power. (a) Dc-bus voltage. (b) Dc-bus current. (c) Decoupled d-q axis currents. (d) Ac side voltage, current responds.

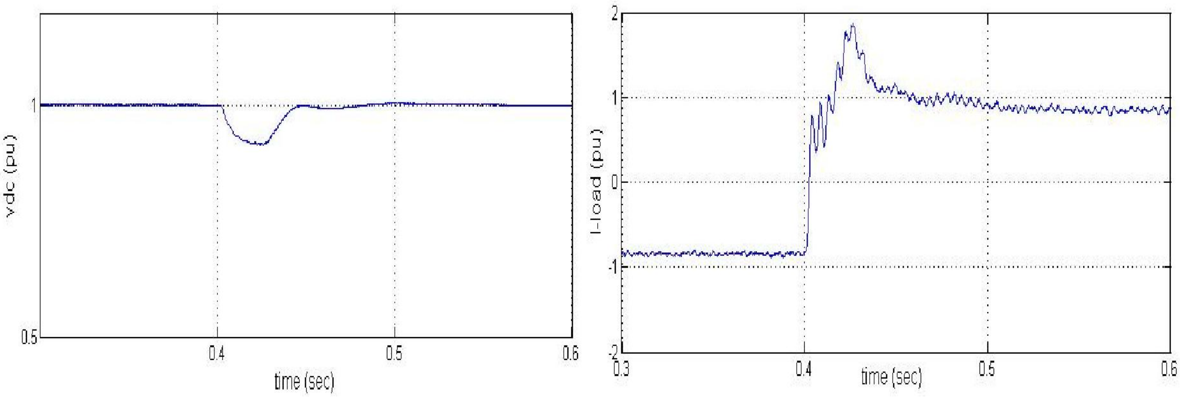

(a) (b)

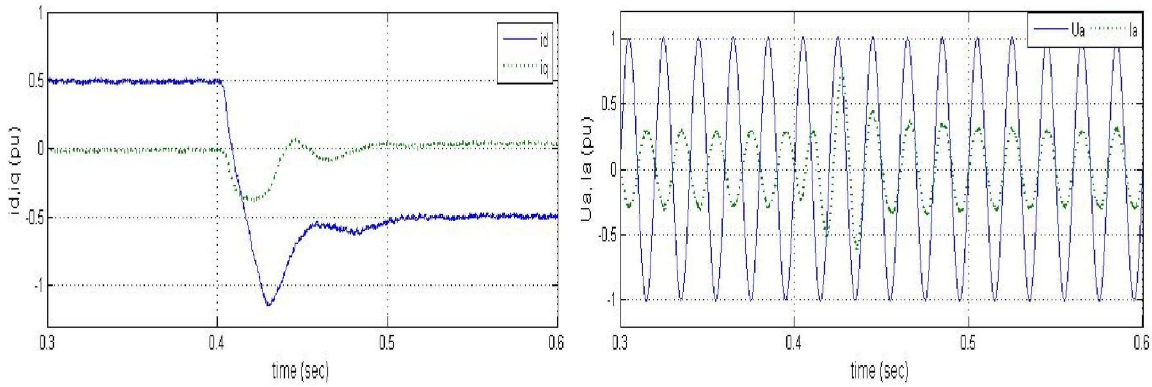

(c) (d)

Fig. 12 Responses to sudden change from rectifying to regenerating mode. (a) Dc-bus voltage. (b) Dc-bus current. (c) Decoupled d-q axis currents (d) Ac side voltage, current responds

Finally, Fig. 13 shows the responses of three-phase to ground fault in the onshore main gird side between 0.4s~0.5s. During an AC fault, the active power exchanged between the converter and the faulty AC system may be significantly reduced owing to the reduced AC voltage and the converter current limit. If the fault is on the AC side of the APC, the delivered power is automatically reduced when the converter reaches its current limit and the DCVC controls the DC voltage by properly reducing the power exchange between the converter and the connected AC system [24] .

7 Conclusion

In this paper, a nonlinear control method based on IOL and zero-dynamic for a VSC-HVDC system has been presented. The nonlinearity of the system

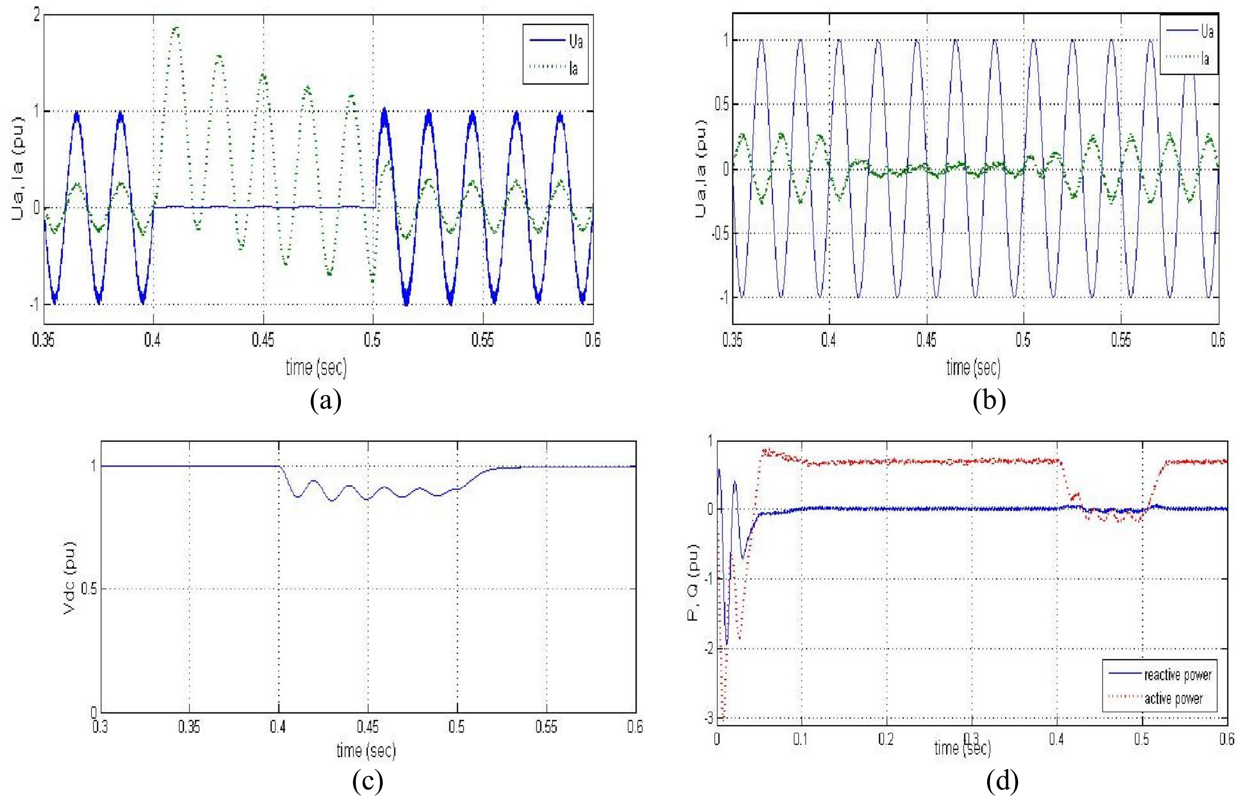

Fig. 13 Waveform of three-phase to ground fault on the grid side. (a) Voltage and current waveform of the offshore wind farm side. (b) Voltage and current waveform of the onshore main grid side. (c) Waveform of the DC bus. (d) Decoupled active and reactive.

and the coupling effect the d-q current control were eliminated by proposed IOL control scheme. By devising the zero dynamics observer in the outer-loop dc-bus voltage controller, the fast zero tracking errors were made, even in the presence of parameter perturbation. The active and reactive power can be independently controlled under unity power factor. Simulations verified the validity and effective of the proposed control scheme which used in VSC-HVDC transmission system. These results show the satisfactory performance of the proposed IOL controller in comparison to the traditional PI controller. Also, the results in this paper can further be an effective scheme in the hardware design of digital control system based on floating point DSP devices.

8 Acknowledgment

This Project was granted financial support from Key Project of National Science Foundation of China (60934005), Shanghai Education Development Foundation (09LM37,10LM26), and Shanghai Scientific Development Foundation (09195802900）.

References:

[1] Dong-Choon Lee, G-Myoung Lee, and K.-D. Lee, DC-Bus Voltage Control of Three-Phase AC DC PWM Converters Using Feedback Linearization, *IEEE Transactions On Industry Applications*, Vol.36, No.3, 2000, pp.826-833.

[2] Niculescu, E., et al., Analysis of PWM converters using MATLAB, *WSEAS Transactions on Circuits and Systems*, 2006. 5(Compendex), pp. 1522-1527.

[3] Carbone, R. and A. Scappatura, An improved three-phase rectifier for PWM adjustable speed drives with passive power factor correction and resistance emulation, *WSEAS Transactions on Circuits and Systems*, 2005. 4(Compendex), pp. 952-959.

[4] Azizi, H., A. Vahedi, and G.H. Papi, Investigation of power quality disturbance effects on the direct power controlled PWM rectifier, *WSEAS Transactions on Systems*, 2005. 4(Compendex), pp. 1777-1784.

[5] Du, C.Q., E. Agneholm, and G. Olsson, VSC-HVDC System for Industrial Plants With Onsite Generators, *IEEE Transactions on Power Delivery*, Vol.24, No.3, 2009, p p. 1359-1366.

[6] Abbas, A.M. and P.W. Lehn, PWM Based

VSC-HVDC Systems - a Review, *2009 Ieee Power & Energy Society General Meeting*, Vol. 1-8, 2009, p p. 4478-4486.

[7] Gonzalez-Hernandez, S., et al., Analysis of Integrated Wind Farm Using a Multiterminal VSC-HVDC: Different Electrical Conditions Response, *2008 40th North American Power Symposium*, 2008, p p. 145-149.

[8] Guedouani Rabea,Fiala Bachir, et al., A new algorithm control for three-phase AC/DC pulse width modulation voltage source rectifier, *WSEAS Transactions on Circuits and Systems,* Vol.6, No.1, 2007, pp.102-109.

[9] Rafiei, Mohammadreza, Ghazi, et al., Robust control methodologies for dc/dc PWM converters under wide changes in operating conditions, *WSEAS Transactions on Systems,* Vol.5, No.11, 2006, pp.2655-2665.

[10] Weixing, L. and O. Boon-Teck, DC overvoltage control during loss of converter in multiterminal voltage-source converter-based HVDC (M-VSC-HVDC), *IEEE Transactions on Power Delivery*, Vol.18, No.3, 2003, pp. 915-920.

[11] Zhou, K.L. and D.W. Wang, Relationship between space-vector modulation and three-phase carrier-based PWM: A comprehensive analysis, *IEEE Transactions On Industrial Electronics*, Vol.49, No.1, 2002, pp. 186-196.

[12] Wang, F., Sine-Triangle versus Space-Vector Modulation for Three-Level PWM Voltage-Source Inverters, *IEEE Transactions On Industry Applications*, VOL.38, NO.2, 2002, pp.500-506.

[13] Jeong, S. and S. Song, Improvement of Predictive Current Control Performance Using Online Parameter Estimation in Phase Controlled Rectifier, *IEEE Transactions On Power Electronics*, Vol.22, No.5, 2007, pp. 1820-1825.

[14] Guedouani Rabea, Fiala Bachir, Berkouk E.M., et al., A new algorithm control for three-phase AC/DC pulse width modulation voltage source rectifier, *WSEAS Transactions on Circuits and Systems,* Vol.6, No.1, 2007, pp.102-109.

[15] Koytiva, X., et al., Application of adaptive fuzzy control for the mitigation of fault disturbances in an HVDC link based on VSCs, *WSEAS Transactions on Systems*, 2005 (Compendex), pp. 1354-1362.

[16] Duarte-Mermoud, Manuel A., Estrada, Jorge L., et al., Model reference adaptive control of linear time-varying plants, *WSEAS Transactions on Circuits and Systems,* Vol.5, No.4, 2006, pp.457-464.

[17] Petrzela Jiri, Hrubos Zdenek, Simplest chaos converters: Modeling, analysis and future perspectives, *Proceedings of the 8th WSEAS International Conference on System Science and Simulation in Engineering, ICOSSSE*, 2009, pp.160-163.

[18] Wang Guo-Qiang, Wang, Zhi-Xin, Control of HVDC-light transmission for offshore wind farms based on input-output feedback linearization and PSO, *WSEAS Transactions on Systems,* Vol.9, No.11, 2010, pp.1109-1119.

[19] Isidori, A., *Nonlinear Control Systems*, Berlin, Germany: Springer-Verlag, 1989.

[20] Slotine, J.E. and W. Li, *Applied Nonlinear Control*, Englewood Cliffs, NJ: Prentice-Hall, 1991.

[21] Daizhan, C., *Applied Nonlinear Control,* China Machine Press, China, 2009.

[22] Tzann-Shin, L., Input-output linearization and zero-dynamics control of three-phase AC/DC voltage-source converters. *IEEE Transactions on Power Electronics,* Vol.18, No.1, 2003, pp.11-22.

[23] Burgos, R.P., E.P. Wiechmann, and J. Holtz, Complex state-space modeling and nonlinear control of active front-end converters, *IEEE Transactions on Industrial Electronics*, Vol.52, No.2, 2005, pp. 363-377.

[24] Moharana, A. and P.K. Dash, Input-Output Linearization and Robust Sliding-Mode Controller for the VSC-HVDC Transmission Link. *IEEE Transactions on Power Delivery*, Vol.25, No.3, 2010, pp. 1952-1961.

[25] Yongsug Suh, Valentin Tijeras, and T.A. Lipo, A Nonlinear Control of the Instantaneous Power in dq Synchronous Frame for PWM AC/DC Converter under Generalized Unbalanced Operating Conditions, *IEEE Industry Applications Society Conference*, Vol.2, 2002, pp.1189-11496.